ISSN 1070-3284, Russian Journal of Coordination Chemistry, 2018, Vol. 44, No. 7, pp. 439–447. © Pleiades Publishing, Ltd., 2018.

Synthesis, Crystal Structure, Luminescence Sensing, and Photocatalytic Properties of a 2D Cobalt(II) Coordination Polymer Containing Bis(benzimidazole) Moieties[1]

X. X. Zhao[a], L. W. Liu[a], Y. F. Li[a], and G. H. Cui[a, *]

[a] *College of Chemical Engineering, Hebei Key Laboratory for Environment Photocatalytic and Electrocatalytic Materials, North China University of Science and Technology, Tangshan, Hebei, 063009 P.R. China*

**e-mail: tscghua@126.com*

Received July 29, 2017

Abstract—A new cobalt(II) coordination polymer, namely $[Co(L)(Ndc)]_n$ (**I**), where L = 1,5-bis(5,6-dimethylbenzimidazole)pentane, H_2Ndc = 2,6-naphthalenedicarboxylic acid, was synthesized and characterized by elemental analysis, IR spectra, powder X-ray diffraction and single-crystal X-ray diffraction (CIF file CCDC no. 1548044). Complex **I** displays a 2D (4,4) layer which further extended into a 3D supramolecular framework via weak C–H···O hydrogen bondings. The luminescence explorations demonstrated that **I** exhibits highly selective and sensitive sensing for $Cr_2O_7^{2-}$ with high quenching efficiency K_{sv} value of 9.87×10^3 L mol^{-1} and low detection limit (0.24 μM ($S/N = 3$)). Meanwhile **I** also exhibits highly selective and sensitive sensing for Fe^{3+} with quenching efficiency $K_{sv} = 3.6 \times 10^4$ L mol^{-1} and low detection limit (0.32 μM ($S/N = 3$)). Complex **I** exhibits higher photocatalytic activities for the degradation of methylene blue under UV irradiation. Additionally, the thermal behavior and electrochemical properties of the compound are also presented.

Keywords: flexible bis(benzimidazole), cobalt(II), crystal structure, luminescent sensing, photocatalytic activity

DOI: 10.1134/S1070328418070060

INTRODUCTION

The designed and construction of coordination polymers (CPs) has been of intense interest, due to their intriguing aesthetic structures and topological features [1], as well as their promising applications in molecular magnetism, molecular sensor, heterogeneous catalysis, drug delivery, molecular sorption and so on [2–6]. Recently, important progress has been achieved in the uses of the luminescence property of CPs for sensing of anions and metal ions [7–10]. Current research indicates that sensors based on luminescent CPs can bring some improvements through their interesting properties, such as real-time monitoring, fast response, high selective sensitivity, etc. With the development of industry, anion pollutants have become more serious environmental problems. As for anion pollutants, dichromic acid with strong oxidizing property has been widely used in leather tanning, detergent and wood preservation, so $Cr_2O_7^{2-}$ anions may appear in the waste water [11, 12]. On the other hand, iron is one of the most abundant elements in humans and animals. Fe^{3+} ions play an important part in many biochemical processes at the cellular level, such as the storage and transport of oxygen, and enzymatic reactions of the mitochondrial respiratory chain. Iron deficiency or excess will lead to many pathological diseases, including skin ailments, hemochromatosis, various anemia, heart failure, and insomnia. Therefore new materials that can quickly and selectively detect $Cr_2O_7^{2-}$ and Fe^{3+} ions have become an urgent need [13].

The increase in the amount of wastewater containing organic dyes led to significant challenges around the world because of their adverse effects on the human health and environment. Organic dye molecules usually involve one or more benzene rings which are hard to be degraded by conventional chemical and biological methods [14]. So far, there are lots of powerful ways to remove organic dyes, for instance, adsorption, precipitation and coagulation [15–17]. However, these conventional techniques have potential limitations because they simply transfer pollutants from one phase to another, or concentrate pollutants in one stage, rather than degrading pollutants. Employ

[1] The article is published in the original.

various coordination polymers as photocatalysis can decompose a wide range of organic pollutants into easily biodegradable compounds or less toxic molecules.

As an important family of multidentate N-donor ligands, flexible bis(benzimidazolyl)alkane derivatives seem to be excellent building blocks as bridging ligands with outstanding coordination ability, due to their reactivity and adaptability in the stabilization of diverse frameworks [18, 19]. And the flexible nature of spacers allows the ligands to bend and rotate when coordinating to metal centers so as to conform to the coordination geometries of metal ions. Additionally, 5,6-dimethylbenzimidazole can serve as an axial ligand for cobalt in the biosynthesis of vitamin B_{12} [20]. As for aromatic multicarboxylic acids, such as 2,6-naphthalenedicarboxylic acid (H_2Ndc), can adopt diversiform bridging/chelating modes, which are beneficial for coordinating with metal centers in the construction of CPs [21]. Until now, the flexible bis(5,6-dimethylbenzimidazole) ligands have been given more and more attention by our and other groups [22–24]. However, coordination polymers based on flexible bis(5,6-dimethylbenzimidazoles) pentane have been rarely studied. Herein, we report synthesis and characterization of a Co(II) coordination compound: $[Co(L)(Ndc)]_n$ (**I**), where L = 1,5-bis(5,6-dimethylbenzimidazole)pentane. We demonstrate here that **I** can be used for detection of $Cr_2O_7^{2-}$ anions and Fe^{3+} ion with high stability, selectivity and sensitivity. In addition, electrochemical property, and photocatalytic behaviors in degrading methyl blue (MB) were introduced in detail.

EXPERIMENTAL

Materials and physical measurements. The L ligand was synthesized according to the literature procedure [25–27]. All reagents and solvents were obtained from Sinopharm Chemical Reagent and used without further purification. Elemental analysis (C, H, and N) was performed with a Perkin-Elmer 240C elemental analyzer. IR spectra were recorded on an Avatar 360 (Nicolet) spectrophotometer using KBr pellets in the range of 4000–400 cm^{-1}. The powder X-ray diffraction data were made on Rigaku D/Max-2500PC X-ray diffractometer with CuK_α radiation (λ = 1.542 Å) and ω–2θ scan mode at 293 K. Thermogravimetric (TG) analysis was performed on a Netzsch STA449 F1 thermogravimetric analyzer from temperature to 800°C with a heating rate of 10°C min^{-1} under nitrogen gas flow of 60 mL min^{-1}. Fluorescence measurements were recorded with a FS5 Edinburgh fluorescence spectrophotometer at room temperature. The solid-state diffuse-reflectance UV-Vis spectra for powder samples were recorded on a UV-Vis spectrometer (Puxi, T9) equipped with an integrating sphere by using $BaSO_4$ as a white standard. A CHI660 electrochemical workstation (Chenhua Instrument, Shanghai, China) was used for control of the electrochemical measurements and data collection. A conventional three-electrode system was used, with a carbon paste electrode (CPE) as a working electrode, a saturated calomel electrode (SCE) as reference electrode, and a platinum electrode as auxiliary electrode.

Synthesis of complex I. A reaction mixture of $CoSO_4 \cdot 7H_2O$ (28.1 mg, 0.1 mmol), H_2Ndc (21.4 mg, 0.1 mmol), the L ligand (36.0 mg, 0.1 mmol), NaOH (8.0 mg, 0.2 mmol), and distilled water (10 mL) was charged into a 25 mL Teflon-lined vessel and reacted at 140°C for 72 h and then naturally cooled to room temperature. Red blocked crystals of **I** were gathered in 38.7% (based on Co).

For $C_{35}H_{34}N_4O_4Co$			
Anal. calcd., %	C, 66.35	H, 5.41	N, 8.84
Found, %	C, 66.11	H, 5.32	N, 8.70

IR (KBr; ν, cm^{-1}): 2918 $\nu(CH_3)$, 1630 $\nu_{as}(COO^-)$, 1559 $\nu_s(COO^-)$, 1508 $\nu(C{=}N)$.

X-ray diffraction determination. Crystallographic data for **I** were carried out using a Bruker SMART 1000 CCD diffractometer with MoK_α radiation (λ = 0.71073 Å) by using an ω scan mode. Data absorption corrections were performed with the SADABS software package [28]. The structure was solved by direct methods using Olex2 software with the SHELXT structure solution program and refined by full-matrix least-squares on F^2 with SHELXL-2016 [29]. Atomic displacements for nonhydrogen atoms were refined using an anisotropic model. All hydrogen atoms are determined by geometric hydrogenation. The detailed crystal structure refinement data are given in Table 1, selected bond lengths and angles are listed in Table 2.

Atomic coordinates and other parameters of complex **I** was deposited with the Cambridge Crystallographic Data Centre (CCDC no. 1548044; deposit@ccdc.cam.ac.ukor http://www.ccdc.cam.ac.uk/conts/retrieving.html).

Fluorescence quenching experiments. All inorganic salts were dissolved in deionized water (100 mL) to afford 10^{-2} mol/L aqueous solutions. The anions solutions were obtained from KNO_3, KCl, KBr, KI, $KClO_3$, $KBrO_3$, KIO_3, and $K_2Cr_2O_7$, and cation solutions were prepared from $Cu(NO_3)_2$, $Al(NO_3)_3$, $Ba(NO_3)_2$, $Cd(NO_3)_2$, $Mg(NO_3)_2$, KNO_3, $Cr(NO_3)_3$, $Fe(NO_3)_3$, $AgNO_3$, $Ca(NO_3)_2$, $Ni(NO_3)_2$, $NaNO_3$, $Pb(NO_3)_2$, $Zn(NO_3)_2$ in the deionized water. Complex **I** (4 mg) was ground into powder and suspended in 4 mL aqueous solutions containing different salt solutions of the same concentration (10^{-2} mol/L), aged for 24 h to form a stable suspension. The emission intensities of these solutions excited by 370 nm were recorded on a fluorescence spectrometer.

Table 1. Crystallographic data and structure refinementsfor **I**

Parameter	Value
Formula weight	633.59
Crystal system	Monoclinic
Space group	*C*2/*c*
a, Å	20.2516(11)
b, Å	13.6049(7)
c, Å	11.6226(6)
β,deg	106.3590(10)
V, Å^3	3072.6(3)
Z	4
ρ_{calcd}, g/cm^3	1.370
Absorption coefficient, mm^{-1}	0.604
F(000)	1324
Crystal size, mm	0.22 × 0.22 × 0.18
θ range for data collection, deg	2.366–28.338
Index range *h*, *k*, *l*	$-26 \le h \le 126$, $-18 \le k \le 18$, $-13 \le l \le 15$
Reflections collected	24187
Independent reflections (R_{int})	3833 (0.0352)
Data/restraint/parameters	3833/0/202
Goodness-of-fit on F^2	1.048
Final R_1, wR_2 ($I > 2\sigma(I)$)	0.0584, 0.1570
Largest diff. peak and hole, *e* Å^{-3}	1.023 and −0.357

Photocatalytic experiments. The photocatalytic activity of **I** as photocatalyst was evaluated by the photodegradation of MB under 500 W Hg lamp irradiation at room temperature in photocatalytic assessment system. A typical process as follows: 0.01 mmol powders of **I** were added into 100 mL of a methylene blue (MB) solution (10 mg L^{-1}). Prior to irradiation, the suspension is magnetically stirred in dark for 60 min to ensure the establishment of an adsorption/desorption equilibrium. 3 mL sample is extracted at 15 min intervals using 5 mL pipettor and centrifuged to remove the residual catalyst. The MB concentration was estimated by the absorbance at 664 nm [30]. Meantime, the control experiment was also accomplished in the following reaction conditions: (a) in the dark with photocatalyst; (b) without photocatalyst under UV irradiation; (c) with photocatalyst under UV irradiation in the presence of tertbutyl alcohol (TBA). The degradation efficiency of MB is defined as follows:

$$\text{Degradation efficiency} = (c_0 - c_t)/c_0 \times 100\%, \quad (1)$$

where c_0 (mg/L) is the initial concentration of MB, and c_t (mg/L) is the concentration of MB at reaction time, *t* (min).

Preparation of CP bulk-modified CPE (1-CPE) was carried outas follows: 0.50 g of graphite powder and 0.03 g of **I** were mixed and ground together ground together with thoroughly using a mortar and pestle. Paraffin oil was then added and continuously mixed until a homogeneous paste was obtained. The homogenized mixture was packed into a teflon tube with 3 mm inner diameter to a length of 10 mm, and the copper wire surface was wiped with emery paper. Then the electrical contact was established with a copper wire [31].

RESULTS AND DISCUSSION

The single-crystal X-ray diffraction analysis reveals that **I** is a 2D coordination polymer. The fundamental building unit of the crystal structure for **I** is composed of half of Co^{2+} ion, a half of L ligand, and a half of anionic Ndc^{2-} ligand, respectively. The Co(II) center is six-coordinated and shows a slightly distorted octahedron geometry (Fig. 1a), ligated by four oxygen atoms belonging to two carboxylate groups from two separated Ndc^{2-} ligands (Co(1)–O(1) 2.079(2), Co(1)–O(2) 2.278(2) Å), and two nitrogen atoms from two separated L ligands (Co(1)–N(2) 2.067(2) Å). The coordination angles range from

Table 2. The selected bond lengths (Å) and angles (deg) for **I***

Bond	*d*, Å	Bond	*d*, Å
Co(1)–O(1)	2.079(2)	Co(1)–O(2)	2.278(2)
Co(1)–N(2)	2.067(2)		
Angle	**ω, deg**	**Angle**	**ω, deg**
N(2*A*)Co(1)N(2)	91.68(1)	N(2*A*)Co(1)O(1)	100.56(9)
N(2*A*)Co(1)O(1*A*)	103.87(1)	O(1)Co(1)O(2)	59.79(9)
O(2*A*)Co(1)O(2)	89.13(1)	O(1)Co(1)O(1*A*)	144.65(1)
N(2*A*)Co(1)O(2*A*)	92.92(1)	N(2*A*)Co(1)O(2)	160.35(9)
O(1)Co(1)O(2*A*)	94.04(9)		

* Symmetry code (*A*): $-x + 1, y, -z + 1/2$.

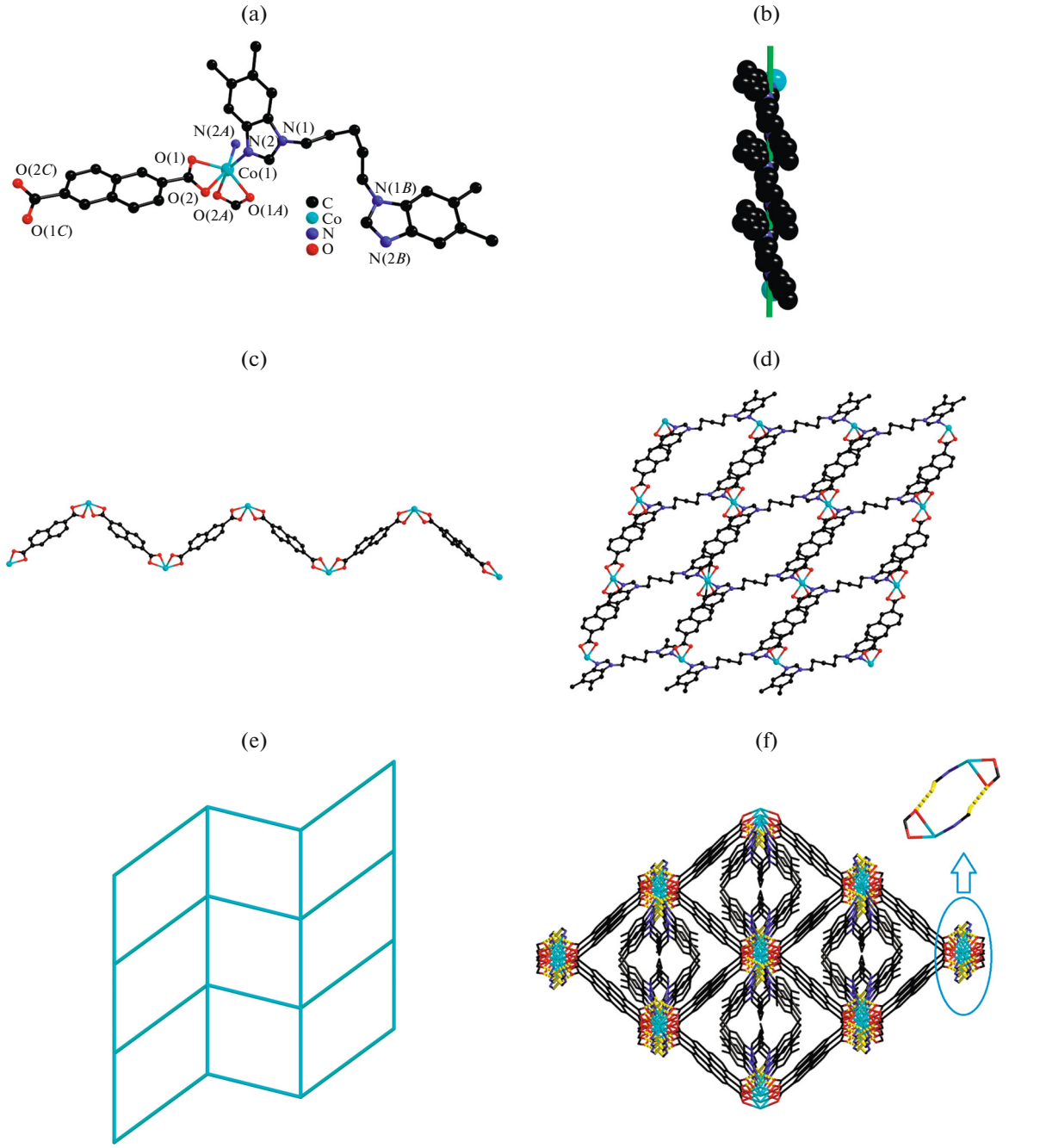

Fig. 1. The coordination environment of Co^{2+} ion in **I** with 30% thermal ellipsoids (hydrogen atoms are omitted for clarity, symmetry codes: (*A*) $-x + 1, y, -z + 1/2$; (*B*) $-x + 1, y, -z + 3/2$; (*C*) $-x + 1/2, -y + 1/2, -z$) (a); the helical chain constructed by Co^{2+} ions and L ligands (b); the 1D zigzag chain constructed by Ndc^{2-} ligands (c); ball-and-stick view of the 2D framework structure in **I** (d); sql topology network of **I** (e); 3D supramolecular framework of **I** constructed by C–H···O hydrogen bonding interactions (f).

59.59(9)° to 160.35(9)°, which are in the normal range of those observed in Co(II)-based CPs [32, 33].

In **I**, the L ligand adopts a *trans*-conformation mode with the dihedral angle between the benzimidazole rings of 55.15(1)° to form a 1D $[Co(L)]_n$ *meso*-helical chain with left-handed helical loops in one single strand and the helical pitch is 11.623(1) Å (Fig. 1b). Moreover, the completely deprotonated Ndc^{2-} ligands employ a $(\kappa^1{-}\kappa^1){-}(\kappa^1{-}\kappa^1){-}\mu_2$ coordination mode to link neighboring Co^{2+} ions, resulting in the formation of 1D $[Co(Ndc)]_n$ zigzag chain with Co···Co distance of 12.899(7) Å (Fig. 1c). Furthermore, two types of 1D

chain are cross-linked with each other to generate a complicated 2D framework with dimensions of 11.623 × 12.899 Å (Fig. 1d). The coordination framework was simplified and analyzed with the Topos 4.0 program package [34]. The network can be simplified as a uninodal (4,4)-connected sql topology with the point symbol of $(4^2 \times 6^2)$, as shown in Fig. 1e. In addition, the 2D framework is further extended by weak C–H···O hydrogen bonding interactions, which results in a 3D supramolecular network (C(7)···O(2) 3.272(4) Å, C(7)–H(7)···O(2) 155°, symmetry code (D): $1 - x$, $1 - y$, $1 - z$) (Fig. 1f).

The main features in the IR spectra of the **I** mainly concern the carboxylate groups and the N-heterocyclic ligands L. For **I**, no strong absorption peaks at 1700 cm^{-1} are observed, indicating that carboxylic groups of Ndc^{2-} are completely deprotonated [35]. The presence of bands at 1508 and 800 cm^{-1} can be assigned to the ν(C=N) (stretching vibration of the L ligands). Characteristic bands at 1630 and 1559 cm^{-1} are due to the vibrations of the carboxylic groups. The value of Δν ($\nu_{as}(COO) - \nu_s(COO)$) is 71 cm^{-1} for **I** that indicates coordination of Ndc^{2-} with cobalt(II) in a chelating bridging mode. The absorption peaks of CH_2 and CH_3 groups in **I** appear at 2918 cm^{-1}. For the purpose of checking the phase purity of **I**, XRD patterns have been checked at ambient temperature. For **I**, the measured XRD patterns agreed well with the calculated from the X-ray single-crystal diffraction data, confirming the phase purity. The slight differences in intensities can be attributed to the preferred orientations of the crystalline powder samples.

TG analysis was carried out to examine the thermal stability **I** under the nitrogen atmosphere. The TG curve showed that **I** is stable up to 350°C. A total weight loss of 87.2% occurred in the temperature range 351–500°C, due to the decomposition of the L and Ndc ligands (calcd. 86.7%). The final residue percentage of 12.8% is consistent with the formation of CoO (calcd. 13.3%) in **I** in the temperature range of 500–800°C.

The luminescence properties of the ligand L and the title **I** were investigated in the solid state at room temperature (Fig. 2). The free ligand L was found to reveal a strong emission at 361 nm on the excitation of 222 nm that is probably attributed to $\pi^* \rightarrow n$ or $\pi^* \rightarrow \pi$ transition [36]. Meanwhile **I** was found to character an emission at 370 nm on the excitation of 216 nm. Comparing with the free L ligand, the emission maximum of **I** is red-shifted by 9 nm, which could be assigned to metal-to-ligand charge-transfer (MLCT) with electrons being transferred from the Co(II) centers to the unoccupied p^* orbitals of the benzimidazolyl groups of L ligand [37].

Complex **I** as the luminescent probe was carefully explored for sensing diverse anions and metal ions. The luminescence behaviors of **I** dispersed in various

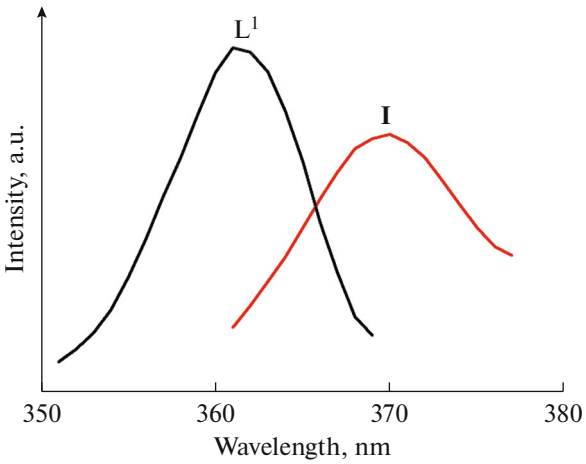

Fig. 2. Solid state emission spectra of free ligand L and **I** at room temperature.

solvents were explored as a suspension after immersion. The solvents included H_2O, methanol (CH_3OH), ethanol (C_2H_5OH), pentanone ($C_5H_{10}O$), ethylene glycol ($(CH_2OH)_2$), dimethyl sulfoxide (DMSO), *n*-butanol ($CH_3(CH_2)_3OH$), dichloromethane (CH_2Cl_2), *N*,*N*-dimethylacetamide (DMA), acetonitrile (C_2H_3N). The chemical stability in different organic solvents was established by soaking **I** in the respective media for 24 h and subsequent XRD analysis. As shown in Fig. 3, the emission intensities at 370 nm for different solvents follow the sequence of H_2O > methanol > ethanol > ethylene glycol > acetonitrile > *n*-butanol > pentanone > dimethyl sulfoxide > *N*,*N*-dimethylacetamide > dichloromethane. Obviously, the solvent molecules exert an influence on the emission of **I**. Upon excitation, the solvent molecules can rearrange according to the excited state dipole vector and stabilize the excited state. The more polar the solvent molecule, the more the excited state is stabilized.

In order to study the luminescent responses to different anions, complex **I** was ground into powder and suspended in aqueous solutions containing different salt solutions of the same concentration (10^{-2} mol/L) of blank, NO_3^-, Cl^-, Br^-, I^-, ClO_3^-, BrO_3^-, IO_3^-, and $Cr_2O_7^{2-}$. As shown in Fig. 4, only $Cr_2O_7^{2-}$ anions gave a significant fluorescence quenching effect, while there was only a negligible effect on the luminescence intensity for other anions. The result indicates the high selectivity of **I** for the detection and specific recognition of $Cr_2O_7^{2-}$ anions in aqueous solutions. Therefore, **I** may be chosen as a candidate for selective sensing of $Cr_2O_7^{2-}$ anions. The result of XRD measurement demonstrates that **I** retains its structural integrity, which indicates that the luminescent quenching could not be attributed to the collapse of the framework.

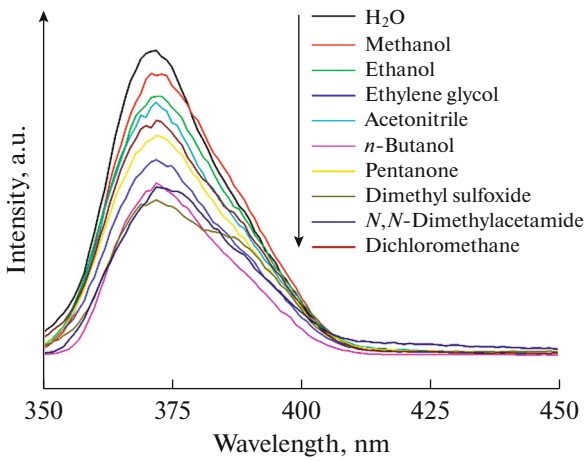

Fig. 3. Emission spectra and emission intensities for **I** in different solvents.

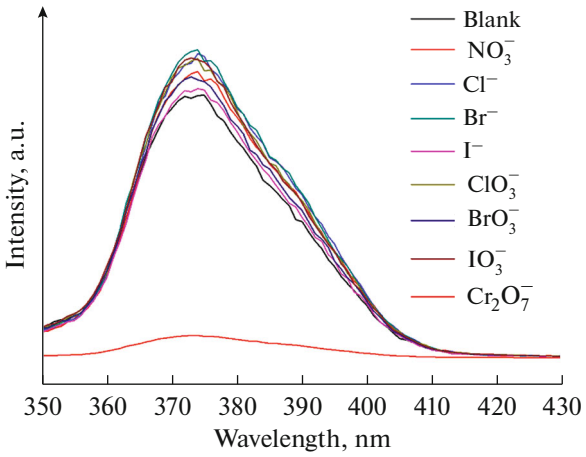

Fig. 4. Comparison of the luminescence intensity of **I** at 370 nm incorporating aqueous solutions (10^{-2} M) upon the addition of various anions.

Moreover, to explore the detection limit of **I** as a luminescent probe for detecting $Cr_2O_7^{2-}$, a series of suspensions of $Cr_2O_7^{2-}$ (5 to 60 μmol/L) were prepared by dropping **I** into the different concentrations of aqueous solution of $Cr_2O_7^{2-}$. It can be seen that, when $Cr_2O_7^{2-}$ concentrations gradually increase, the fluorescent intensity of **I** gradually decreases (Fig. 5a). The luminescence intensity linearly decreases with the concentration of $Cr_2O_7^{2-}$ varying from 5 to 60 μmol/L. The detection limit of **I** as a luminescent probe for detecting $Cr_2O_7^{2-}$ is supported by the calculated results based on the equation: detection limit = $3\sigma/k$ (σ is the standard deviation of blank measurement; k represents the slope between the luminescence intensity vs. log[$Cr_2O_7^{2-}$]. To further investigate the correlation between the quenching effect and $Cr_2O_7^{2-}$ concentration, the linear luminescence intensity vs. $Cr_2O_7^{2-}$ concentration plot was made (Fig. 5b), which can be fitted through the equation $I_0/I = 1 + K_{sv}[Cr_2O_7^{2-}]$ (I_0 and I are the fluorescent intensities of **I** before and after adding $Cr_2O_7^{2-}$, respectively; K_{sv} is the quenching rate constant; [$Cr_2O_7^{2-}$] represents the concentration of $Cr_2O_7^{2-}$). The K_{sv} value is calculated to be 9.87×10^3 L mol^{-1}, indicating the high quenching-efficiency constant of $Cr_2O_7^{2-}$ in the emission of **I**. The high quenching efficiency and low detection limit of 0.24 μmol/L ($S/N = 3$) also reveal that **I** can act as visually luminescent probes for discrimination and detection of $Cr_2O_7^{2-}$ anions.

At the same time, the strong luminescence of **I** and good water stabilities promoted us to investigate their potential applications in the detection of metal cations. Their luminescent intensities are significantly dependent on the loaded metal cations. Luminescence intensities of **I** exist significant quenching effects when loaded Fe^{3+} ions, whereas other metal ions exhibit no quenching effects (Fig. 6). The XRD patterns of the Fe^{3+} loaded **I** were nearly the same as those of original samples. The results demonstrate that their basic frameworks remain unchanged after loaded Fe^{3+} ions. To further evaluate the sensitivity of luminescence quenching by Fe^{3+} in detail, studies were performed for **I** by monitoring a series of suspensions with gradually increasing Fe^{3+} concentration. As shown in Figs. 7a, 7b, the emission intensities of **I** were all gradually weakened with the increasing of Fe^{3+} from 5 to 60 μmol/L. Via the luminescent data, the K_{sv} were calculated as 3.6×10^4 L mol^{-1}. The high sensitivities and low detection limits (0.32 μmol/L ($S/N = 3$)) demonstrate that **I** can be highly effective and selective luminescent sensors for Fe^{3+} ions.

Since the title compound is insoluble in water and common organic solvents, a bulk modified CPE is the optimal choice to study its electrochemical properties [38]. It is well-known that the scan rate has a remarkable influence on the electrochemical properties. The cyclic voltammograms for 1-CPE in 1 M H_2SO_4 aqueous solution at different scan rates are presented in Fig. 8. It can be seen clearly that one reversible redox peak (I–I') appears in the potential range from +0.18 to +0.36 V, which should be ascribed to the redox of Co(III)/Co(II) [39, 40]. The mean peak potential $E_{1/2} = (E_{pa} + E_{pc})/2$ is 0.26 V. It can be seen in Fig. 8 that as the scan rates increase from 0.04 to 0.5 V s^{-1}, the reduction peak potentials shifted to the negative direction and the relevant oxidation peak potentials shifted to the positive direction and the peak currents

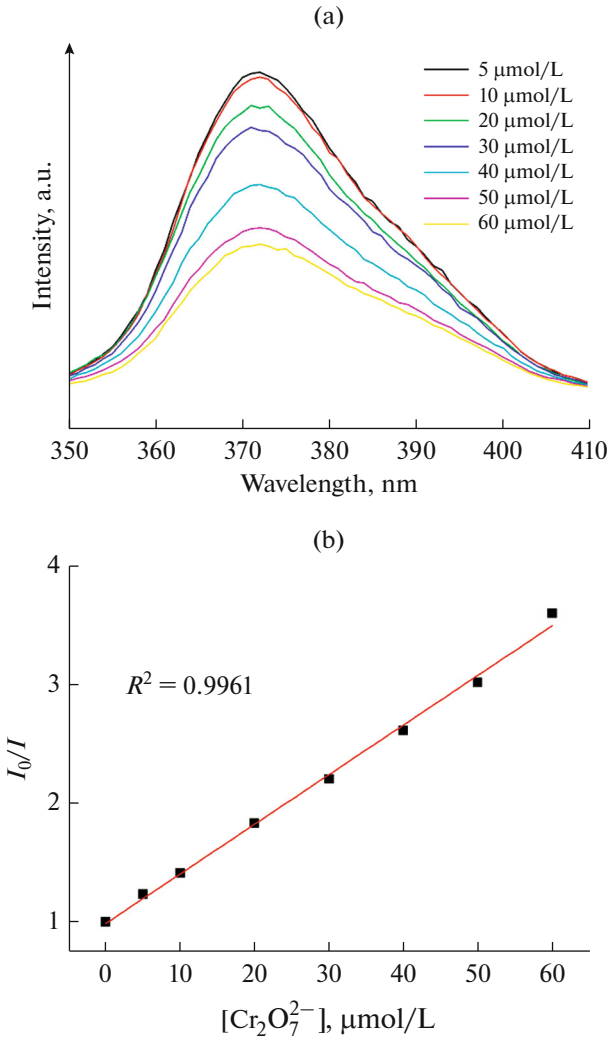

Fig. 5. Luminescence spectra of **I** under different concentrations of $Cr_2O_7^{2-}$ aqueous solutions (a) and linear luminescence intensity vs. $Cr_2O_7^{2-}$ concentration plot (b).

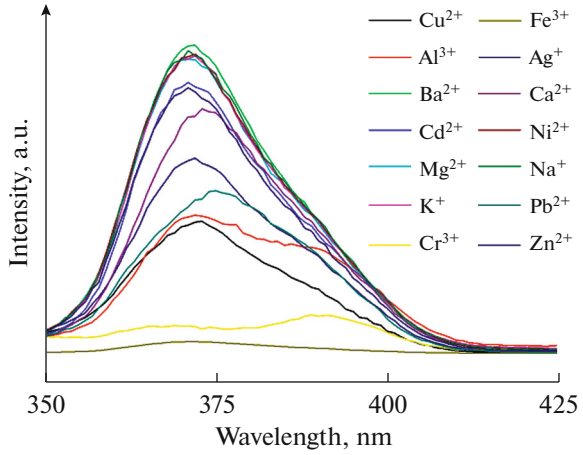

Fig. 6. Emission spectra for **I** in solutions of different metal cations.

are proportional to the scan rates, which indicates the redox process of Co-CPE is surface-controlled [41].

The main reason for the UV-Vis absorption spectrum is the change in the electron energy level in the molecule, which is caused by the valence electrons in the compound molecules from the low energy level to the high energy level transition. The characteristic curve mainly embodies the intrinsic regularity of the valence electrons in the transition between the corresponding energy levels. Herein, we investigated the solid state absorption spectra of **I** at room temperature. The main absorption bands of the **I** were at 290 and 540 nm, which could be ascribed to metal-to-ligand charge transfer (MLCT) and *d*–*d* spin-allowed transition of the Co^{2+} (d^7) ions, respectively [42]. The measurement of UV-Vis diffuse reflectivity for a powder sample was used to obtain its optical band gap E_g. The optical absorption associated with E_g can be assessed at 3.51 eV for **I**, which illustrates the presence of an optical band gapand the nature of semiconductivity for **I**. Therefore, **I** possesses possible potential for UV-light photocatalytic activity.

In the process of photocatalytic degradation, the organic dye chromophore is damaged and broken down into nonpolluting small molecules [43]. Herein, MB as a kind of dye contaminant is selected to evaluate the photocatalytic effectiveness in the purification of wastewater. The absorption peak of MB decreased obviously with the increasing reaction time for **I** under UV irradiation (Fig. 9). Furthermore, no other new peaks are observed in Fig. 9, indicating that no new pollutants occurred during the process of degradation. The catalytic activities of **I** are monitored by measuring their maximum absorbance at $\lambda_{max} = 664$ nm, the color of the solution change obviously in which MB changes from blue to light blue or even colorless, the degradation efficiency of MB reaches 86.8% after 105 min. When **I** was placed into an aqueous solution of the MB in a dark environment for 105 min, there is no obvious decrease in the absorbance value, which may avoid the possibility of adsorbing such a dye molecule into the frameworks and the catalytic degradation efficiency of MB is only 6.6%. By contrast, only 13.6% MB was degraded in the absence of photocatalyst under UV irradiation.

In order to study the photocatalytic mechanism, TBA, a widely used $^{\bullet}OH$ radical scavenger, was used in the photodegradation experiment [44, 45]. The photocatalytic efficiency decreased obviously from 86.8 to 51.2%, proving that the TBA can greatly depress the photodegradation of MB solution with **I**. It is well known that there is an electron transfer from the highest occupied molecular orbital (HOMO) to the lowest unoccupied molecular orbital (LUMO) in the presence of UV light. The HOMO is mainly contributed by

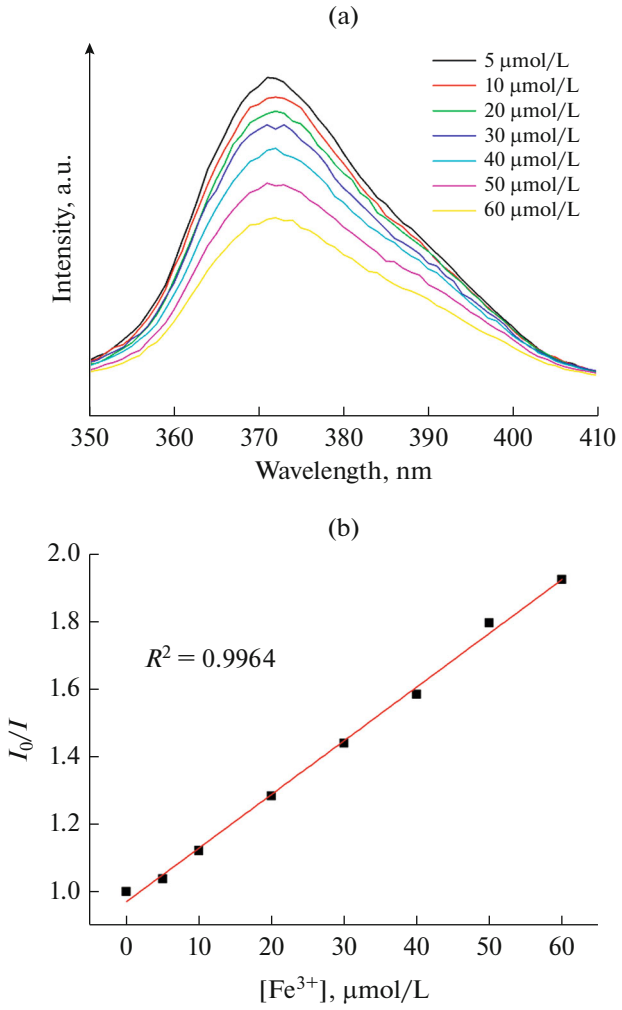

Fig. 7. Luminescence spectra of **I** under different concentrations of Fe^{3+} aqueous solutions (a) and linear luminescence intensity vs. Fe^{3+} concentration plot (b).

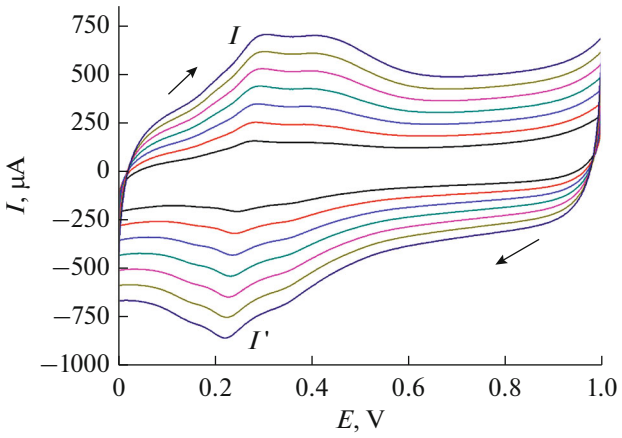

Fig. 8. Cyclic voltammograms for 1-CPE in 1 M H_2SO_4 solution at different scan rates.

O and/or N2*p* bonding orbitals, and the LUMO is mainly contributed by empty M orbitals [46]. Once in the presence of UV light, there will appear electron transfer from the HOMO to LUMO. The electron of the excited state in LUMO is usually very easy to lose, and HOMO strongly urges one electron to return to its steady state. Thus, an electron is trapped from the water molecule and oxidized to the •OH active material. Then, •OH can effectively decompose MB to complete the photocatalytic process.

To quantify the reactions the kinetic data for the degradation of MB under UV light irradiation can be fitted by the pseudo-first-order rate equation. This can be written as $\ln(c_0/c) = kt$, where k is the rate constant, c and c_0 are the concentration of MB at irradiation time $t = t$ and 0, respectively. The rate constant for CP is found to be 0.0206 min^{-1}. However, the rate constants of control experiment are 0.0006, 0.0013, and 0.0068 min^{-1}, respectively. Additionally, when MB was re-added in the system, the photocatalytic activity of Co(II) in **I** did not decrease significantly after four runs of photocatalytic experiments. The results suggest that **I** possess good photocatalytic activity and stability for photodegradation of MB.

In summary, a six-coordinated cobalt(II) coordination polymer has been hydrothermally synthesized. Complex **I** exhibits helical chain with left-handed helical loops and extends into 3D supramolecular frameworks via hydrogen bonding interactions. Luminescence measurements illustrate that **I** shows highly sensitive response to $Cr_2O_7^{2-}$ and Fe^{3+} ions. Complex **I** exhibits good activities and stabilities for the photocatalytic decomposition of MB dyes. Moreover, the catalyst of **I** is easy to be recycled considering it is insoluble in water solution.

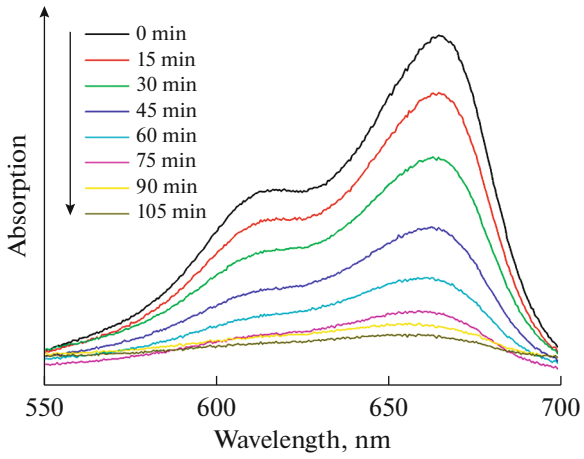

Fig. 9. Absorption spectra of the MB solution during the decomposition reaction under UV light irradiation with the use of **I**.

ACKNOWLEDGMENTS

The project was supported by the National Natural Science Foundation of China (51474086), Natural Science Foundation–Steel and Iron Foundation of Hebei Province (B2015209299).

REFERENCES

1. Kumar, V., Pilati, T., Terraneo, G., et al., *Chem. Sci.*, 2017, vol. 8, p. 1801.
2. Bar, A.K., Pichon, C., and Sutter, J.P., *Coord. Chem. Rev.*, 2016, vol. 308, p. 346.
3. Hu, M., Belik, A.A., Imura, M., et al., *J. Am. Chem. Soc.*, 2013, vol. 135, p. 384.
4. Hou, Y.L., Sun, R.W., Zhou, X.P., et al., *Chem. Commun.*, 2014, vol. 50, p. 2295.
5. Stylianou, K.C., Warren, J.E., Chong, S.Y., et al., *Chem. Commun.*, 2011, vol. 47, p. 3389.
6. Chen, D.M., Tian, J.Y., Fang, S.M., et al., *Inorg. Chem. Commun.*, 2016, vol. 66, p. 69.
7. Shustova, N.B., Cozzolino, A.F., Reineke, S., et al., *J. Am. Chem. Soc.*, 2013, vol. 135, p. 13326.
8. Li, H.Y., Wei, Y.L., Dong, X.Y., et al., *Chem. Mater.*, 2015, vol. 27, p. 1327.
9. Tian, A., Ning, Y., Yang, Y., et al., *Dalton Trans.*, 2015, vol. 44, p. 16486.
10. Xiang, Z.H., Fang, C.Q., Leng, S.H., et al., *J. Mater. Chem.*, 2014, vol. 2, p. 7662.
11. Kieber, R.J., Willey, J.D., and Zvalaren, S.D., *Environ. Sci. Technol.*, 2002, vol. 36, p. 5321.
12. Li, L.L., Fan, L.L., Sun, M., et al., *Colloids Surf., B*, 2013, vol. 107, p. 76.
13. Kovalchuk, A., Bricks, J.L., Trieflinger, C., et al., *J. Am. Chem. Soc.*, 2005, vol. 127, p. 13522.
14. Wang, C.C., Li, J.R., Lv, X.L., et al., *Energy Environ. Sci.*, 2014, vol. 7, p. 2831.
15. Zhu, M.X., Lee, L., Wang, H.H., et al., *J. Hazard. Mater.*, 2007, vol. 149, p. 735.
16. Zhao, L., Ma, J., and Sun, Z.Z., *Appl. Catal., B*, 2008, vol. 79, p. 244.
17. Li, Y., Cui, W., Liu, L., et al., *Appl. Catal., B*, 2016, vol. 199, p. 412.
18. Wang, X.L., Hou, L.L., Zhang, J.W., et al., *Inorg. Chim. Acta*, 2013, vol. 405, p. 58.
19. Jing, W., Ren, Z.G., Dai, M., et al., *CrystEngComm*, 2011, vol. 13, p. 5111.
20. Marwaha, S.S., Sethi, R.P., and Kennedy, J.F., *Enzyme Microb. Technol.*, 1983, vol. 5, p. 361.
21. Liu, Q.Y., Wang, W.F., Wang, Y.L., et al., *J. Tang Inorg. Chem.*, 2012, vol. 51, p. 2381.
22. Jiao, C.H., He, C.H., Geng, J.C., et al., *J. Coord. Chem.*, 2012, vol. 65, p. 2852.
23. Liu, G.C., Yang, S., Wang, X.L., et al., *Russ. J. Coord. Chem.*, 2012, vol. 38, p. 55. doi 10.1134/S1070328411120050
24. Liu, G.C., Huang, J.J., Zhang, J.W., et al., *Transition Met. Chem.*, 2013, vol. 38, p. 359.
25. Aakeröy, C.B., Desper, J., Elisabeth, E., et al., *Z. Kristallogr.*, 2005, vol. 220, p. 325.
26. Zhang, X., Zhao, Y.Q., Wang, F.S., et al., *Chin. J. Struct. Chem.*, 2016, vol. 35, p. 765.
27. Hao, S.Y., Hao, Z.C., Liu, Y.G., et al., *Chin. J. Struct. Chem.*, 2017, vol. 36, p. 118.
28. Pal, A., Debreczeni, J.E., Sevvana, M., et al., *Acta Crystallogr., Sect. D: Biol. Crystallogr.*, 2008, vol. 64, p. 985.
29. Sheldrick, G.M., *Acta Crystallogr., Sect. C: Struct. Chem.*, 2015, vol. 71, p. 3.
30. Jing, H.P., Wang, C.C., Zhang, Y.W., et al., *RSC Adv.*, 2014, vol. 4, p. 54454.
31. Kuwana, T. and French, W.G., *Anal. Chem.*, 1964, vol. 36, p. 241.
32. Hao, S.Y., Hou, S.X., Van Hecke, K., et al., *Dalton Trans.*, 2017, vol. 46, p. 1951.
33. Cui, J.W., Hou, S.X., Van Hecke, K., et al., *Dalton Trans.*, 2017, vol. 46, p. 2892.
34. Blatov, V.A., Shevchenko, A.P., and Proserpio, D.M., *Cryst. Growth Des.*, 2014, vol. 14, p. 3576.
35. Hao, J.M., Yu, B.Y., Van Hecke, K., et al., *CrystEngComm*, 2015, vol. 17, p. 2279.
36. Wang, X.X., Yu, B., Van Hecke, K., et al., *RSC Adv.*, 2014, vol. 4, p. 61281.
37. Rosa, A., Ricciardi, G., Baerends, E.J., et al., *J. Phys. Chem.*, 1996, vol. 100, p. 15346.
38. Han, Z.G., Zhao, Y.L., Peng, J., et al., *Electroanal.*, 2005, vol. 17, p. 1097.
39. Meghdadi, S., Mereiter, K., Mohammadi, N.S., et al., *Inorg. Chem. Res.*, 2016, vol. 1, p. 69.
40. Wang, X.L., Mu, B., Lin, H.Y., et al., *Dalton Trans.*, vol. 41, p. 11074.
41. Wang, X.L., Gao, Q., Tian, A.X., et al., *J. Solid State Chem.*, 2012, vol. 187, p. 219.
42. Wen, L.L., Zhao, J.B., Lv, K.L., et al., *Cryst. Growth Des.*, 2012, vol. 12, p. 1603.
43. Liu, B., Yu, Z.T., Yang, J., et al., *Inorg. Chem.*, 2011, vol. 50, p. 8967.
44. Wen, L.L., Wang, F., Feng, J., et al., *Cryst. Growth Des.*, 2009, vol. 9, p. 3581.
45. Chen, J., Wen, W., Kong, L., et al., *Ind. Eng. Chem. Res.*, 2014, vol. 53, p. 6297.
46. Wang, C.C., Zhang, Y.Q., Zhu, T., et al., *Desalin. Water Treat.*, 2015, vol. 57, p. 17844.